Chinese Chemical Letters 37 (2026) 112068

Contents lists available at ScienceDirect

Chinese Chemical Letters

journal homepage: www.elsevier.com/locate/cclet

FeB-activated peracetic acid for carbamazepine degradation: Generation of multiple reactive oxygen species and a two-stage activation mechanism

Jiali Peng[a,1], Yu Mei[a,1], Shihuai Deng[a,*], Yanjun Li[a], Chenye Fu[a], Yi Ren[b], Guochun Lv[a], Zehua Wang[c], Xiaoxun Xu[a], Xiaohui Lu[a,*], Bo Lai[d]

[a] College of Environmental Sciences, Sichuan Agricultural University, Chengdu 611130, China
[b] State Key Laboratory of Hydraulics and Mountain River Engineering, College of Water Resource & Hydropower, Sichuan University, Chengdu 610065, China
[c] School of Eco-Environment, Hebei University, Baoding 071002, China
[d] Department of Environmental Science and Engineering, School of Architecture and Environment, Sichuan University, Chengdu 610065, China

ARTICLE INFO

Article history:
Received 11 June 2025
Revised 27 August 2025
Accepted 5 November 2025
Available online 12 November 2025

Keywords:
peracetic acid
Hydrogen peroxide
Iron boride
Segmentation mechanism
Selective oxidation
Fe(III)/Fe(II) cycling

ABSTRACT

Recently, iron-based heterogenous catalysts have attracted widespread attention in the activation of peracetic acid (PAA) for generating reactive oxygen species (ROS) to degrade pollutants. However, in heterogeneous PAA activation systems, the role of coexisting H_2O_2 in PAA is often overlooked. To clarify the dynamic roles of both PAA and H_2O_2, herein, iron boride (FeB) was employed as a heterogeneous activator of PAA for carbamazepine (CBZ) degradation. The generation of high valent iron (Fe(IV)), hydroxyl radicals (•OH) and organic radicals (RO•) in the FeB/PAA system were identified through quenching experiments, electron paramagnetic resonance (EPR) spectroscopy, and semi-quantitative analysis. At the initial stage of the reaction, the active sites of FeB preferentially reacted with PAA, rather than H_2O_2, primarily generating Fe(IV) to oxidize CBZ. Subsequently, PAA was gradually depleted, dissolved Fe(II) slowly released from FeB reacts with H_2O_2 in the solution to generate •OH. Besides, density functional theory (DFT) calculations and masking experiments revealed that the surface Fe(II) (≡Fe(II)) acts as the dominant active center for PAA activation. Moreover, the selective oxidation of various pollutants by these ROS is governed by the differing sensitivities of the contaminants to ROS. The electron-donating B–B bonds in FeB can effectively promote the Fe(III)/Fe(II) redox cycling, exhibiting exceptional catalytic performance. Additionally, the possible degradation pathways of CBZ were proposed by combining ultra-performance liquid chromatography coupled with quadrupole time-of-flight mass spectrometry (UPLC-QTOF-MS/MS) and DFT calculations. This work provides new insights into the activation mechanism of PAA by FeB, offering a sustainable and efficient approach for the treatment of emerging pollutants.

© 2026 Published by Elsevier B.V. on behalf of Chinese Chemical Society and Institute of Materia Medica, Chinese Academy of Medical Sciences.

Advanced oxidation processes (AOPs) are promising treatment techniques for the removal of emerging contaminants through the activation of various oxidants, including hydrogen peroxide (H_2O_2), persulfate (PS), and peracetic acid (PAA) [1–3], rely on the generation of reactive oxygen species (ROS). PAA, in particular, has gained significant attention due to its high redox potential (1.06−1.96 V) and minimal formation of toxic by-products [4], making it a promising alternative to traditional oxidants like H_2O_2 and PS in degrading recalcitrant organic contaminants. Additionally, the O–O bond energy in PAA (159 kJ/mol) is significantly lower than that in H_2O_2 (213 kJ/mol) and peroxymonosulfate (PMS, 317 kJ/mol) [5], which facilitates easier activation and enhances its efficiency in AOPs.

Although PAA is a strong oxidant thermodynamically, it also fails to degrade refractory pollutants when used alone [6]. Therefore, a variety of strategies for activating PAA have been proposed to achieve efficient degradation of pollutants by generating active species (*e.g.*, hydroxyl radicals (•OH) and organic radicals (RO•)) with strong oxidation capacity. Specifically, UV irradiation, ultrasound, and metal ions (*e.g.*, Mn(II), Fe(II), Cu(II), and Ru(III)) have been widely studied for PAA activation [7,8]. Among these, Fenton and Fenton-like systems are widely studied for their high efficiency and cost-effectiveness [9,10]. For instance, the Fe^{2+}/PAA system

* Corresponding authors.
E-mail addresses: shdeng@sicau.edu.cn (S. Deng), lxh1993@sicau.edu.cn (X. Lu).
[1] These authors contributed equally to this work.

https://doi.org/10.1016/j.cclet.2025.112068
1001-8417/© 2026 Published by Elsevier B.V. on behalf of Chinese Chemical Society and Institute of Materia Medica, Chinese Academy of Medical Sciences.

achieves micropollutant degradation with apparent rate constants (k_{app}) ranging from 1.10×10^5 L mol^{-1} s^{-1} to 1.56×10^4 L mol^{-1} s^{-1} [11]. However, homogeneous systems face inherent limitations, including metal sludge accumulation, high reagent consumption, and secondary pollution risks (*e.g.*, toxic Co^{2+} leaching in Co^{2+}/PAA systems) [12]. In light of this, it is essential to develop heterogeneous catalysts for the activation of PAA.

Unlike homogeneous ions, heterogeneous catalysts can be easily recovered and reused, making the heterogeneous reaction more promising for water purification applications [13]. Fe-based catalysts are more attractive due to their abundant geological reserves, low cost, and environmental friendliness, which are widely considered one of the best-performing catalysts in activating chemical oxidants for degrading organic pollutants in water [14,15]. Nevertheless, the majority of existing typical Fe-based catalysts (*e.g.*, zero-valent iron, iron oxides and iron oxychlorides) exhibit limited acid resistance and thus have poor stability under typical acidic conditions. Meanwhile, most iron-based catalysts cannot achieve an efficient Fe(II)/Fe(III) redox cycle and thus exhibit a low catalytic activity [16]. Previous studies have reported that boron possesses a strong electron-donating ability to regenerate Fe(II) and therefore assist Fe-based AOPs optimization [17,18]. As a boron-based material, iron boride (FeB), consisting of Fe(0) and B(0), can promote the conversion of Fe(III) to Fe(II) and thereby optimizing catalytic performance. Moreover, FeB, synthesized from low-cost and abundant elements *via* simple solid-state reactions, is a cost-effective catalyst with reductive sites that enhance iron-catalyzed Fenton-like reactions. Furthermore, FeB can be considered for PAA activation because it requires no intensive energy input, avoids secondary pollution, and exhibits magnetic properties that facilitate easy recycled. Notably, H_2O_2 inevitably coexist with PAA in solution. While previous studies have demonstrated that H_2O_2 plays a significant role in homogeneous PAA activation systems [19,20], whereas its contribution in heterogeneous PAA activation remains largely unexplored, particularly in systems involving Fe-based catalysts with redox-active sites like FeB. Consequently, developing FeB as a heterogeneous catalyst is an effective strategy to expand the application of PAA oxidation systems in wastewater treatment, while helping to elucidate the overlooked role of H_2O_2 in heterogeneous PAA activation processes.

In this work, FeB was applied for the activation of PAA to degrade carbamazepine (CBZ). The objectives of this work are: (i) To evaluate the degradation performance of the FeB/PAA system towards CBZ degradation; (ii) to elucidate the generation of primary ROS and their reactivity toward various pollutants; (iii) to explore the catalytic mechanism under the coexistence of H_2O_2 and PAA; (iv) to investigate the role of boron in facilitating the iron cycle from the perspective of multi-dimensional characterization; (v) to identify the degradation intermediates and degradation pathways for CBZ abatement and elucidate the toxicity of the degradation products. This research provides a promising and innovative strategy for wastewater treatment, addressing the limitations of conventional wastewater processes regarding inefficient micropollutant removal.

The used chemicals and reagents are listed in Text S1 (Supporting information).

Experiments were conducted in 200 mL of reaction solution containing 20 μmol/L CBZ at 30 °C, with initial pH adjusted using NaOH/H_2SO_4. Reactions were initiated by adding PAA and FeB under mechanical stirring (300 r/min). Samples were collected at intervals, filtered through a 0.22 μm polytetrafluoroethylene membrane, and quenched with 20 μL of 0.1 mol/L $Na_2S_2O_3$. All experiments were performed at least two times and the error bars of standard deviation and average value were given.

The characterizations and analytical methods are stated in Texts S2-S12 (Supporting information).

As shown in Fig. S1a (Supporting information), CBZ removal was slightly removed by FeB alone and PAA alone but could be completely degraded within 45 min by coupling FeB and PAA, suggesting the effectiveness of PAA activation by FeB. Notably, the catalytic performance of other boron-based and iron-based materials for degradation decreased in the sequence: FeO > WB > MOB = Fe_2O_3 > Fe^0 > B_4C > B > B_2O_3, further indicating the excellent activation performance of FeB on PAA activation (Figs. S1b and S2 in Supporting information). Besides, the effects of crucial reaction parameters were then explored in the FeB/PAA system, including PAA concentrations (Fig. S1c in Supporting information), FeB dosages (Fig. S1d in Supporting information), and solution pH, more details are provided in Texts S13 and S14 (Supporting information). Moreover, the H_2O_2 and CH_3COO^- in PAA solution played a negligible role in eliminating CBZ in the FeB/PAA system (Figs. S3 and S4 in Supporting information).

It is reported that various ROS including $^{\bullet}OH$, $RO^{\bullet}$, singlet oxygen ($^1O_2$), superoxide radical ($^{\bullet}O_2^-$), and high-valent iron (Fe(IV)) can be generated in iron-based PAA system *via* complicated radical chain reactions (Eqs. 1−7) [21]. The specific $RO^{\bullet}$, such as $CH_3C(O)O^{\bullet}$, $CH_3C(O)OO^{\bullet}$, $CH_3^{\bullet}$ and $CH_3O_2^{\bullet}$, are always produced through the activation of PAA by the heterogeneous catalysts.

Consistent with these reports, premixing experiments demonstrated varying degrees of CBZ degradation inhibition at different premixing durations, indirectly confirming the crucial role of short-lived ROS in pollutant degradation in the FeB/PAA system (Fig. S5 in Supporting information). In order to elucidate the types and contributions of ROS in the FeB/PAA system, the effect of different radical scavengers such as methanol (MeOH), *tert*–butanol (TBA), 2,4-hexadiene (2,4-HD) and Mn^{2+} on CBZ abatement were studied. MeOH is an effective quenching agent for $^{\bullet}OH$, $RO^{\bullet}$ and Fe(IV) [22]. As can be seen from Fig. S6 (Supporting information), CBZ abatement was inhibited by 91.5 % in the presence of 4 mmol/L MeOH, when the concentration was added to 100 mmol/L, the CBZ removal was fully suppressed. The significant inhibitory effect of MeOH on CBZ abatement can be explained as the contributions of $^{\bullet}OH$, $RO^{\bullet}$ and Fe(IV). TBA is a typical scavenger for $^{\bullet}OH$ [7]. Fig. 1a demonstrated that 100 mmol/L TBA strongly inhibited about 71 % of CBZ degradation, confirming that $^{\bullet}OH$ was one of the critical ROS. Subsequently, 2,4-HD, an effective quencher capable of scavenging both $^{\bullet}OH$ and $RO^{\bullet}$, was adopted further to evaluate the relative contributions of ROS (Fig. 1a) [23]. The CBZ removal was obviously hampered in the presence of 2,4-HD, and it is clearly shown that only 27.8 % of CBZ was degraded with 10 mmol/L 2,4-HD. Furthermore, Zhang *et al.* [8]. discovered that Mn^{2+} could effectively quench $CH_3C(O)OO^{\bullet}$ through electron transfer without interfering with PAA decomposition. As illustrated in Fig. S7 (Supporting information), 1 mmol/L Mn^{2+} inhibited about 95.5 % of CBZ degradation, confirming that $CH_3C(O)OO^{\bullet}$ as the dominant $RO^{\bullet}$ species contributing marginally to CBZ degradation. Moreover, superoxide dismutase (SOD) is a typical $^{\bullet}O_2^-$ quenching reagent that can be used to analyze $^{\bullet}O_2^-$ generated in the FeB/PAA system [24]. As demonstrated in Fig. 1a, the effect of SOD on CBZ degradation was negligible, indicating that $^{\bullet}O_2^-$ could not participate in the CBZ removal. Through the above quenching experiments, it was found that the inhibitory effect of 10 mmol/L 2,4-HD was comparable with 100 mmol/L TBA, while 100 mmol/L MeOH exhibited the strongest inhibition. The quenching results of 2,4-HD and TBA demonstrated that $RO^{\bullet}$ played a limited role in CBZ degradation, whereas $^{\bullet}OH$ contributed more significantly. The comparative analysis of quenching effects between 2,4-HD and MeOH further confirmed the evident contribution of Fe(IV) species.

Furthermore, PMSO was chosen as the chemical probe to qualitatively and semi-quantitatively disclose the generation of Fe(IV) since the distinctive interaction between PMSO and Fe(IV) to produce $PMSO_2$ by an oxygen transfer route [25]. As illustrated in Fig.

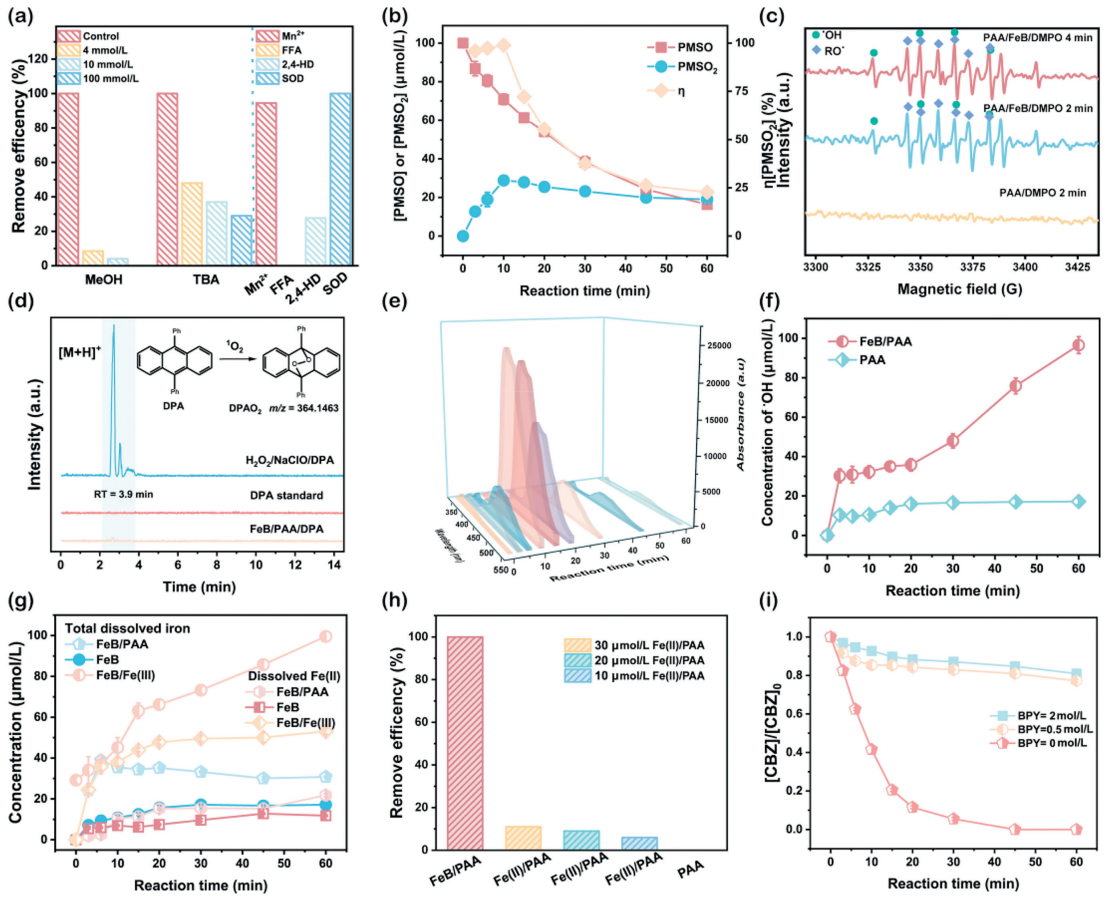


Fig. 1. (a) Removal of CBZ degradation by different radical scavengers in the FeB/PAA system. (b) Change in concentrations of PMSO and $PMSO_2$ and $\eta(PMSO_2)$ in the FeB/PAA system. (c) EPR spectra of DMPO adduct in the FeB/PAA and PAA systems (conditions: 0.2 g/L FeB, 800 μmol/L PAA, [DMPO] = 10 mmol/L). (d) EIC of $DPAO_2$ generated in the NaClO/H_2O_2 and FeB/PAA systems (conditions: [DPA] = 60 mmol/L, NaClO = 1 mg/L, H_2O_2 = 9.8 mol/L). (e) The fluorescence signal peak of 7-HOC in the FeB/PAA. (f) Semi-quantitative analysis of •OH in FeB/PAA mediated systems with BA as a probe. (g) Concentrations of dissolved Fe(II) and total dissolved iron in different FeB systems. (h) Effect of different concentrations of Fe(II) coupled to PAA on CBZ degradation. (i) Effect of BPY on CBZ degradation in FeB/PAA system. Conditions: 20 μmol/L CBZ, 0.1 g/L FeB, 300 μmol/l PAA, pH_0 5.6 and T = 30 °C, Mn^{2+} = 1 mmol/L, FFA = 100 mmol/L, SOD = 50 U/L, PMSO = 100 μmol/L, BA = 3 g/L, coumarin = 20 μmol/L.

1b, the concentrations of PMSO and $PMSO_2$ exhibited a complementary relationship, with the $\eta(PMSO_2)$ (defined as the ratio of formed $PMSO_2$ to consumed PMSO) close to 100 % during the initial 10 min of the reaction. Interestingly, we observed that PMSO continued to be consumed after 10 min, while the generation of $PMSO_2$ did not further increase and even exhibited a slight decline, leading to a significant decline of $\eta(PMSO_2)$. The decrease of $\eta(PMSO_2)$ can be attributed to two main factors. On the one hand, PMSO reacted with •OH and was transformed into other by-products, contributing to its enhanced consumption. On the other hand, the generated $PMSO_2$ could undergo further degradation in the FeB/PAA system, as shown in Fig. S8 (Supporting information). Consequently, the actual $\eta(PMSO_2)$ is likely underestimated due to the additional degradation of $PMSO_2$. In conclusion, the results imply that the amount of Fe(IV) generated in the FeB/PAA system was limited in the later stages of the reaction, with its dominant contribution mainly concentrated in the first 10 min of the reaction.

$$CH_3C(O)OOH + Fe(II) \rightarrow CH_3C(O)O^{\bullet} + Fe(III) + OH^- \quad (1)$$

$$CH_3C(O)OOH + CH_3C(O)O^{\bullet} \rightarrow CH_3C(O)OO^{\bullet} + CH_3C(O)OH \quad (2)$$

$$CH_3C(O)OOH + Fe(II) \rightarrow CH_3C(O)O^- + Fe(III) + {}^{\bullet}OH \quad (3)$$

$$CH_3C(O)OOH + Fe(II) \rightarrow CH_3C(O)OH + Fe^{IV}O^{2+} \quad (4)$$

$$CH_3C(O)OOH + CH_3C(O)OO^- \rightarrow CH_3C(O)O^- + CH_3C(O)OH + {}^1O_2 \quad (5)$$

$$CH_3C(O)OO^{\bullet} \rightarrow HO_2^{\bullet} + CH_2CO^{\bullet} \quad (6)$$

$$CH_3C(O)O^{\bullet} \rightarrow CH_3^{\bullet} + CO_2 \quad (7)$$

Moreover, to investigate the role of $^1O_2$ in the FeB/PAA system, furfuryl alcohol (FFA), a typical $^1O_2$ quencher, was applied (Fig. 1a) [26]. Although the addition of FFA significantly inhibited CBZ removal in the FeB/PAA system, the relatively weak oxidation potential of $^1O_2$ renders its contribution to pollutant degradation controversial [27]. Thus, quenching experiments cannot directly indicate the contribution of $^1O_2$ and further investigation is required.

To further verify the existence of •OH, RO• and $^1O_2$, electron paramagnetic resonance (EPR) tests were performed by using 5,5-dimethyl-1-pyrroline *N*-oxide (DMPO) and 2,2,6,6-tetramethylpiperidine (TEMP) as the spin trapping agents. As depicted in Fig. 1c, a significant signal with a peak intensity ratio of 1:2:2:1 (indicated by the green round shape), which was consistent with the DMPO–•OH adduct, implying the possible generation of •OH in the FeB/PAA system. At the same time, the characteristic peaks of DMPO–RO• spin adducts (indicated by the purple diamond shape) also were observed [28]. As for $^1O_2$, TEMP

was employed as a spin trap to detect $^1O_2$. TEMP is oxidized by $^1O_2$ and forms 2,2,6,6-tetramethyl-piperidinyl-1-oxy (TEMPO), which can be identified *via* EPR spectroscopy as a 1:1:1 triplet signal. As shown in Fig. S9 (Supporting information), the triplet signal of $^1O_2$ was detected in both the FeB/PAA system and the PAA alone system with comparable peak intensities, indicating that FeB did not enhance the production of $^1O_2$. Previous studies have reported that using TEMP to detect $^1O_2$, other reactive oxygen species (*e.g.*, $^{\bullet}OH$) or high-valent metals such as Fe(VI)/Fe(V)/Fe(IV)) may oxidize TEMP to TEMPO *via* hydrogen atom transfer pathways and generates EPR signals resembling the characteristic 1:1:1 triplet of $^1O_2$, leading to false-positive results [29]. Furthermore, almost all $^1O_2$ were deactivated by water and hardly oxidized micropollutants in non-photochemical systems, considering the high deactivation rate constant of $^1O_2$ in water [30]. Therefore, the above results suggest that $^1O_2$ is unlikely to contribute significantly to CBZ degradation.

To provide direct evidence for $RO^{\bullet}$ and $^1O_2$ generated in the FeB/PAA system, the TEMPO and 9,10-diphenyl anthracene (DPA) were further employed as a probe to capture $RO^{\bullet}$ and $^1O_2$ [31], respectively, and detected *via* quadrupole time-of-flight mass spectrometry (UPLC-QTOF-MS/MS). Fig. S10 (Supporting information) shows that signals of $CH_3C(O)O-$TEMPO adduct (*m/z* 216.1) were successfully detected [32]. In addition, $CH_3C(O)O^{\bullet}$ could rapidly decompose to generate $CH_3^{\bullet}$ *via* Eq. 7 and the signal of CH_3-TEMPO (*m/z* 172.1) was also observed in the UPLC-QTOF-MS/MS spectra. From Fig. 1d and Fig. S11 (Supporting information), $NaClO/H_2O_2$, as a typical system that could produce $^1O_2$ [33], we successfully detected $DPAO_2$ (*m/z* 364.14), a product of DPA oxidized by $^1O_2$. However, no $DPAO_2$ was detected in the FeB/PAA/DPA system, which could exclude the production of $^1O_2$. Moreover, for the direct evidence of the existence of $^{\bullet}OH$, it is extensively considered that $^{\bullet}OH$ could react with coumarin to generate 7-hydroxycoumarin (7-HOC) *via* H-abstraction thus the generation of $^{\bullet}OH$ can also be detected using coumarin. Fig. 1e shows the obvious peak of the fluorescence signal in the FeB/PAA system. These results demonstrate that $^{\bullet}OH$, $RO^{\bullet}$ (primarily $CH_3C(O)O^{\bullet}$ and $CH_3C(O)OO^{\bullet}$) and Fe(IV) were produced in the FeB/PAA system.

In an attempt to identify the contribution of $^{\bullet}OH$ in-depth, benzoic acid (BA) was used as a chemical probe to semi-quantitative to detect the concentration of $^{\bullet}OH$ since excess BA could capture the $^{\bullet}OH$ to generate hydroxybenzoic acids (HBAs) (*e.g.*, 4-hydroxybenzoic acid (*p*-HBA), 3-hydroxybenzoic acid (3-HBA), 2-hydroxybenzoic acid (SA) and 3,4-dihydroxybenzoic acid (3,4-DHBA)) [34]. While *p*-HBA was the only detectable intermediate in the FeB/PAA system, its concentration has been used to estimate cumulative $^{\bullet}OH$ production. The reaction rate constant of BA with $^{\bullet}OH$ is 4.2×10^9 L mol^{-1} s^{-1}, and per mole *p*-HBA was generated quantitatively by 5.87 ± 0.18 mol $^{\bullet}OH$, the cumulative production of $^{\bullet}OH$ could be quantitatively estimated from the concentration of *p*-HBA formed [35]. As depicted in Fig. 1f, 16.45 μmol/L *p*-HBA was accumulated in the FeB/PAA system after 60 min, corresponding to an $^{\bullet}OH$ yield of 96.54 μmol/L, which is significantly higher than that of the PAA alone system.

Based on the analysis of various ROS, the contribution of $^{\bullet}OH$, $RO^{\bullet}$ and Fe(IV) in the FeB/PAA system was demonstrated. Interestingly, we found that Fe(IV) played a more significant role in the first 10 min of the reaction, while $^{\bullet}OH$ tended to be more active in the later stage. A stepwise degradation mechanism was reasonably proposed for the FeB/PAA system. To investigate this segmented mechanism deeply, TBA as a quencher of $^{\bullet}OH$ was introduced into the PMSO conversion experiment at 10 min [36]. As shown in Fig. 1b and Fig. S12 (Supporting information), compared to the PMSO conversion experiment conducted without TBA, the $\eta(PMSO_2)$ was nearly identical within the first 10 min. However, after 100 mmol/L TBA was introduced, the concentration of PMSO remained stable, indicating that PMSO was no longer oxidized by $^{\bullet}OH$ present in the system. Furthermore, there is no evidence to suggest that PMSO undergoes an oxidation reaction with $RO^{\bullet}$. Therefore, we are more inclined to propose that the subsequent consumption of PMSO is attributed to its oxidation by $^{\bullet}OH$. Additionally, ATZ is a pollutant that can be easily degraded by $^{\bullet}OH$ [37], and the effect of TBA on its degradation was also investigated. As shown in Fig. S13 (Supporting information), the degradation rates within the first 10 min were similar in FeB/PAA systems with and without 100 mmol/L TBA. However, in the later stages, the group with 100 mmol/L TBA showed a noticeable inhibition in degradation, which further demonstrates the role of $^{\bullet}OH$ in the later phase of the reaction.

Later, the change in the concentration of PAA and H_2O_2 in the FeB/PAA system also were observed. The dynamic competition between H_2O_2 and PAA in the FeB/PAA system was revealed through their concentration changes (Fig. S14 in Supporting information). During the initial rapid reaction phase, PAA was decomposed faster than H_2O_2, which demonstrated that PAA has superior reactivity toward FeB than H_2O_2. Thus, during the initial phase, the reaction of PAA with FeB predominates, yielding Fe(IV) that serves as the primary ROS for CBZ degradation.

In addition, the changes in concentrations of total dissolved iron and dissolved Fe(II) in FeB, FeB/Fe(III) and FeB/PAA systems were investigated. As shown in Fig. 1g, the concentrations of total dissolved iron and dissolved Fe(II) increased in all systems. Notably, in the FeB/PAA system, the total dissolved iron concentration exhibited a rapid increase within the first 10 min, followed by a gradual decline to a stable level of approximately 30 μmol/L. This observation aligns with the proposed two-stage degradation mechanism. It also can be found that the addition of FeB to Fe(III) visibly accelerated the production of Fe(II) and the total dissolved iron, demonstrating the remarkable Fe(III) reduction capacity of FeB (Fig. 1g). To investigate the role of dissolved Fe(II), we added Fe(II) to the PAA system, and the addition of 30 μmol/L Fe(II) resulted in 11 % CBZ removal (Fig. 1h). Furthermore, considering the gradual generation of dissolved Fe(II) in the FeB/PAA system, 30 μmol/L Fe(II) was added in three equal aliquots (10 μmol/L each) to the PAA and H_2O_2 systems. A sharp increase in the CBZ degradation rate was observed immediately after each Fe(II) addition. It was interesting to find that the Fe(II)/H_2O_2 system demonstrates significantly superior efficacy in CBZ degradation compared to Fe(II)/PAA systems, indicating that the Fenton reaction between dissolved Fe(II) and H_2O_2 might play a critical role (Fig. S15a in Supporting information). Therefore, based on the above results, a possible two-stage mechanism can be proposed. In the initial stage, PAA preferentially reacts with FeB to generate Fe(IV), leading to the degradation of CBZ. In the subsequent stage, the concentration of PAA decreased, the dissolved Fe(II) reacted with H_2O_2 *via* the Fenton reaction to produce $^{\bullet}OH$, which further oxidized CBZ (Fig. S16 in Supporting information) (Eqs. 8 and 9).

$$H_2O_2 + Fe^{2+} \rightarrow Fe^{3+} + {}^{\bullet}OH + OH^- \quad (8)$$

$$H_2O_2 + Fe^{3+} \rightarrow Fe^{2+} + HO_2^{\bullet} + H^+ \quad (9)$$

$$B_2O_3 + 3H_2O \rightarrow 2H_3BO_3 \quad (10)$$

$$B + 3Fe(III) + 3H_2O \rightarrow H_3BO_3 + 3Fe(II) + 3H^+ \quad (11)$$

Moreover, Fe(III) was also added to the PAA and H_2O_2 system to investigate the role of Fe(III). As illustrated in Fig. S15b (Supporting information), the removal rate of CBZ is less than 10 %, indicating that the activation of both PAA and H_2O_2 by Fe(III) is nearly negligible. Although Fe(III) exhibits negligible activation capacity toward oxidants, it may play a role in iron redox cycling. In the FeB/PAA

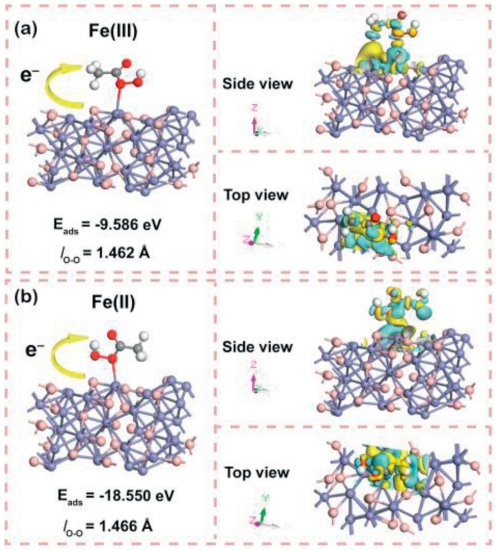


Fig. 2. Charge differential density distribution of (a) Fe(III) and (b) Fe(II) site adsorbed on the PAA.

system, Fe(III) originates from two primary pathways. On the one hand, the structural breakdown or surface corrosion of FeB directly releases Fe(III) into the aqueous phase. On the other hand, Fe(II) species present in solution undergo rapid oxidation by ROS, forming Fe(III) as a product of iron redox cycling. To further elucidate the role of Fe(III) in iron cycling, the combined state of iron species in the solution was analyzed using the Visual MINTEQ database. As shown in Fig. S17 (Supporting information), the iron species predominantly exists as $FeOH^{2+}$ and $Fe(OH)^{2+}$ at pH 4.0 (the introduction of PAA triggers an initial pH shift, followed by stabilization), respectively. As illustrated in Fig. S16 (Supporting information), the iron species amalgamate with FeB as two distinct Fe(III) precursors at a pH of 4.0 within the solution: B atoms may participate in electron-sharing, forming bonds with the electron-deficient Fe(III) atom and the electron-abundant oxygen atom present in $FeOH^{2+}$ (33.6 %) and $Fe(OH)_2^+$ (66.1 %), respectively. In the process, as the B-Fe bonds breaks, the B-B bonds in FeB might act as electron donors, and Fe(II) (exists as Fe^{2+}) is produced *via* a one-electron transfer and subsequently released to the solution to decompose H_2O_2 and produce ROS. Additionally, the electron-deficient B combines with the electron-rich O, initially forming B_2O_3 on the surface of FeB, which is then rapidly reduced in the solution to form boric acid (Eqs. 10 and 11). Furthermore, the reacted FeB can also reduce Fe(III) to Fe(II) in a similar manner, promoting the Fenton cycle until all of it is converted into B_2O_3 and subsequently into boric acid. Even though B_2O_3 hinders the reduction of Fe(III) by blocking the interaction between active boron species and Fe(III) [18], the rapid transformation of borides into boric acid ensures the continuous dissolution of boron, which inherently promotes the sustained reduction of Fe(III). However, the role of B-B bonds requires further verification through subsequent material characterization technique.

The contributions of both dissolved Fe(II) and dissolved Fe(III) species derived from FeB has been validated. To further elucidate the roles of surface Fe(II) (≡Fe(II)) and surface Fe(III) (≡Fe(III)), we performed density functional theory (DFT) calculations. During activation, ≡Fe(III) and ≡Fe(II) exhibited preferential coordination with specific oxygen sites on PAA (Figs. S18 and S19 in Supporting information). Here, we systematically compare the adsorption configurations of PAA on FeB materials with ≡Fe(III) and ≡Fe(II) sites, aiming to elucidate the dominant active center and its mechanism. Fig. 2 revealed that ≡Fe(II) sites exhibited a more negative adsorption energy ($E_{ads} = -18.550$ eV) compared to ≡Fe(III) ($E_{ads} = -9.586$ eV). Also, the O–O bond length of ≡Fe(III) and ≡Fe(II) were 1.462 Å and 1.466 Å, respectively. The longer O–O bond was easier to break, which was favorable for the cleavage of PAA [38,39]. This confirmed that ≡Fe(II) was the primary active sites for PAA activation. Moreover, charge density difference maps of the two models showed that the electron transfer process was more significant when the ≡Fe(II) site adsorbed PAA compared to the ≡Fe(III) sites. Consequently, the ≡Fe(II) site appeared to be the primary reactive site for PAA activation.

To further assess the activation of PAA by ≡Fe(II), 2,2'-bipyridyl (BPY) was introduced into the reaction system since BPY can chelate Fe(II), inhibiting electron transfer to the oxidants on the surface of particles but cannot directly quench •OH. It was a foregone conclusion that the degradation of CBZ decreased from 100 % to 22.8 % in the presence of 0.5 mmol/L BPY (Fig. 1i), revealing the substantial contribution of ≡Fe(II). These results indicate that ≡Fe(II) played a more significant role in the FeB/PAA system, particularly during the initial stage where it reacts with PAA to generate Fe(IV).

Degradation experiments on diverse micropollutants (SMX, BPA, ATZ, NB, SIZ, ACP, CBZ, NAP, PMSO) in the FeB/PAA system revealed that FeB alone exhibited negligible removal efficiency except for NB (33.5 %), which can attributed to the fact that NB is easily reduced by FeB due to its greater reductivity compared to other contaminants [40], while PAA alone was ineffective for all contaminants (Fig. S20 and Fig. S21a in Supporting information). In contrast, the FeB/PAA system achieved high removal efficiencies within 60 min (100 % for SIZ, ACP, CBZ, NAP, PMSO; 93.3 % for BPA; 89.5 % for NB; 87.2 % for ATZ; 61.25 % for SMX), confirming its broad applicability. Notably, degradation efficiency and reactive oxygen species (ROS) contributions varied significantly across pollutants. Quenching experiments demonstrated that •OH dominated degradation of pollutants with electron-deficient aromatic rings (*e.g.*, CBZ, SMX, ATZ, NB; ≈60 % inhibition by TBA), whereas NAP degradation relied heavily on RO• and Fe(IV) (80.4 % inhibition by MeOH), linked to its electron-rich features [28,41,42]. For SIZ, steric hindrance restricted oxidation solely to Fe(IV) (Figs. S21b and S22 in Supporting information) [41]. These systematic differences indicate that pollutant structural properties critically govern their sensitivity to ROS.

The reusability and stability of FeB in PAA activation were evaluated through consecutive cycle tests. Notably, the inherent magnetic properties of FeB make it very convenient to recycle. As shown in Fig. 3a, the CBZ degradation maintained a removal rate of over 80 % after five consecutive runs, demonstrating that the FeB exhibits excellent reusability and stability towards PAA activation. However, the CBZ degradation efficiency gradually decreased with each cycle, especially the second cycle. The observed decline in performance could be attributed to the progressive oxidation of FeB and partial leaching of active components during repeated reactions (Text 16 in Supporting information) [43]. To restore FeB activity, the used FeB after five cycles was regenerated *via* acid pickling. The CBZ removal efficiency increased to over 90 % within 60 min, indicating that acid pickling method might help re-expose the passivated active sites on the surface of FeB, thereby restoring activity.

In order to illuminate the cause of FeB deactivation cycling test, a series of characterization methods were conducted. high-resolution transmission electron microscope (HRTEM) showed fresh FeB possessed crystalline lattice fringes (0.362 nm spacing), while reacted samples exhibited blurred or ambiguous structures indicating oxidation-induced crystallinity loss (Figs. S23a-d in Supporting information). Scanning electron microscope (SEM) reveals that fresh FeB polyhedral particles with smooth surfaces transitioned to porous or loose structures after reaction, confirming morphological corrosion that explains the cycling test results (Figs.

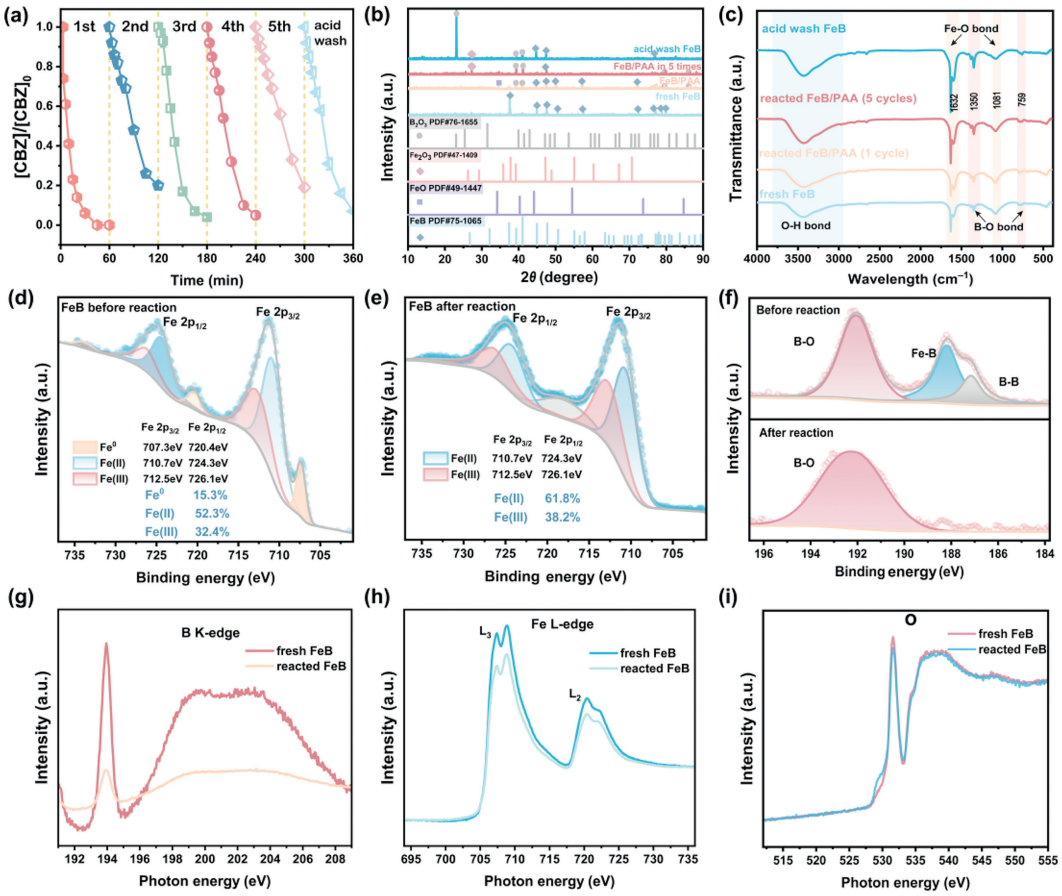


Fig. 3. (a) Reusability of FeB for CBZ removal in the FeB/PAA system. (b) XRD spectrum of fresh and reacted FeB. (c) FT-IR spectra of fresh and reacted FeB. Fe 2p high-resolution spectra of (d) fresh FeB and (e) reacted FeB. (f) B 1s high resolution spectra of fresh FeB and reacted FeB. (g) B K-edge XAS spectra of fresh FeB and used FeB. (h) FeB L-edge XAS spectra of fresh FeB and used FeB. (i) O XAS spectra of fresh FeB and used FeB. Conditions: 0.1 g/L FeB, 300 μmol/L PAA, 20 μmol/L CBZ, pH_0 5.6 and $T = 30$ °C.

S23e and f, S24 and Text S16 in Supporting information). Energy dispersive spectrometer (EDS) elemental mapping demonstrated uniform distribution but substantial compositional shifts of Fe and O increased by 5.22% and 10.8% respectively, while boron decreased by 15.92%, indicating that FeB was oxidized (Figs. S23g-i and m in Supporting information).

Subsequent in-depth characterization analysis revealed the deactivation of FeB stems from structural oxidation and boron depletion during reaction, detailed analysis is provided in Text S16. X-ray diffraction (XRD) confirmed retained bulk crystallinity but detected new low-activity iron and boron oxides (FeO, Fe_2O_3, B_2O_3) after reaction (Fig. 3b). Fourier transform infrared spectroscopy (FT-IR) verified surface oxidation through intensified hydroxyl (3430 cm^{-1}), Fe-O (1632 and 1081 cm^{-1}) and B-O (1350 and 759 cm^{-1}) (Fig. 3c). Critically, XPS revealed that Fe^0 was disappeared completely while Fe(II) and Fe(III) increased to 61.8% and 38.2%, respectively (Figs. 3d and e and Fig. S25 in Supporting information), and B-B/Fe-B bonds disappeared as B_2O_3 increased from 49.2% to 100% (Fig. 3f). Moreover, control experiments confirmed the essential role of B-B bonds in Fe(III)/Fe(II) cycling in the second stage of reaction (Fig. S26 in Supporting information). X-ray absorption spectroscopy (XAS) showed the coordination structure of B has changed and iron valence elevation, consistent with oxide generation (Figs. 3g-i).

To sum up, the FeB/PAA system operates through synergistic homogeneous-heterogeneous activation pathways dominated by ≡Fe(II). The initial phase constitutes the dominant CBZ degradation phase, where ≡Fe(II) reacts with PAA to generate Fe(IV), thereby driving rapid pollutant removal. The subsequent dissolved Fe(II) enables homogeneous Fenton reactions, generating ·OH for secondary degradation. Furthermore, the B-B bonds act as electron donors, promoting the Fe(II)/Fe(III) redox cycle. These results also explain the superior catalytic performance of FeB compared to other iron-based catalysts (Fig. S1b). Thus, FeB is a dual-function catalyst in which ≡Fe(II) primarily activates PAA, while B-mediated electron transfer sustains the iron cycle.

To illuminate the degradation pathways of CBZ, the intermediates generated in the FeB/PAA system were detected by UPLC-QTOF-MS/MS. Moreover, the Fukui index could indicate the potential atoms for electrophilic attack (f^-) and radical attack (f^0) [44], displaying the active sites of CBZ for radicals (Fe(IV), ·OH, RO·) attack. Twelve major intermediates were identified, and their specific information was summarized in Table S1 and Fig. S27 (Supporting information). Based on the identified intermediates and Fukui index, some possible degradation pathways for CBZ were proposed in Fig. 4. Firstly, the alkene double bond in the nitrogenous central heterocycle of CBZ was attacked by reactive radicals especially at C22 and C25, marked with blue circles in Fig. S28 (Supporting information). Sites with higher f^- were most sensitive to ·OH attack, readily transforming monohydroxylated CBZ (*m/z* 253.0933). It may exist as a multiple isomers (**P1**, **P2**, **P3**), which has been reported to be due to the symmetrical structure of CBZ [45]. **P1** undergoes a hydroxylation reaction on the benzene ring under further attack by ·OH to generate **P4** (*m/z* 269.0908). Then **P4** through C–C cleavage to generate **P7** (*m/z* 271.1050). **P2** continued to be oxidized to generate **P5** (*m/z* 251.0824). The aldehyde group in **P5**

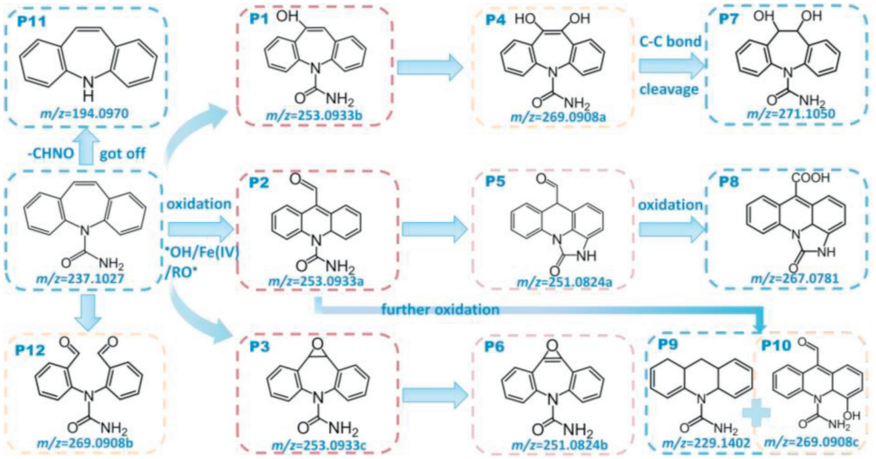


Fig. 4. Proposed pathways of CBZ degradation by the FeB/PAA process.

(*m/z* 251.0824) was converted into a carboxyl group, under the oxidation of Fe(IV), •OH and RO•, to form **P8** (*m/z* 267.0781), which tends to accumulate since it is resistant to oxidation. In addition, the **P2** could undergo further conversion, leading to aldehyde cleavage and ultimately forming **P9** (*m/z* 229.1412) and **P10** (*m/z* 269.0908). **P3** was transformed to **P6** (*m/z* 251.0824). Besides, CBZ can undergo molecular transformation through two distinct pathways: (1) cleavage of the -CHNO moiety to form fragment **P11** (*m/z* 194.0970), and (2) scission of the acetyl-aldehyde group yielding product **P12** (*m/z* 269.0908). The toxicity assessment of CBZ and transformation products was conducted and detailed are stated in Texts 17 and 18, Fig. S29 and Fig. S30 (Supporting information).

This study employed FeB as a heterogeneous catalyst to efficiently activate PAA for the degradation of various organic pollutants in wastewater. Based on quenching, EPR and probe experiments, Fe(IV) and •OH were identified as primary ROS, and two-stage reaction process was involved in the FeB/PAA system. In the reaction system where H_2O_2 and PAA coexist, the active sites of FeB preferentially react with PAA, rather than H_2O_2, generating Fe(IV) for the degradation of CBZ. However, after the depletion of PAA, the dissolved Fe(II) released from FeB reacted with the remaining H_2O_2 *via* a Fenton reaction, generating •OH. DFT calculations and BPY masking experiments revealed that ≡Fe(II) acted as the dominant active center for PAA activation. Besides, due to the differences in the structural properties of various pollutants, their sensitivities to ROS vary, resulting in the selective oxidation of different pollutants by ROS in the FeB/PAA system. Additionally, FeB showed excellent reusability and stability, and the electron-donating B–B bonds in FeB effectively promoted the Fe(III)/Fe(II) redox cycling, achieving persistent and efficient contaminants oxidation. The possible degradation pathways of target CBZ and toxicity assessment of the formed intermediates were also explored in depth. In summary, this study provides novel insights into FeB/PAA system, offering a green and innovative strategy for wastewater treatment.

Declaration of competing interest

The authors declare that they have no known competing financial interests or personal relationships that could have appeared to influence the work reported in this paper.

CRediT authorship contribution statement

Jiali Peng: Writing – review & editing, Writing – original draft, Funding acquisition, Conceptualization. **Yu Mei:** Writing – original draft, Visualization, Methodology, Data curation. **Shihuai Deng:** Writing – review & editing, Supervision, Resources. **Yanjun Li:** Visualization, Data curation. **Chenye Fu:** Visualization, Data curation. **Yi Ren:** Validation, Supervision, Conceptualization. **Guochun Lv:** Software. **Zehua Wang:** Visualization, Software. **Xiaoxun Xu:** Supervision, Resources. **Xiaohui Lu:** Writing – review & editing, Resources, Funding acquisition, Conceptualization. **Bo Lai:** Supervision, Methodology, Conceptualization.

Acknowledgments

The authors would like to acknowledge the financial support from National Science Foundation of China (Nos. 22206139, 22306134, 52000158), Natural Science Foundation of Sichuan Province (Nos. 2024NSFSC1153 and 2025ZNSFSC0958), the China Postdoctoral Science Foundation (No. 2023M732499) and the Postdoctoral Fellowship Program of CPSF.

Supplementary materials

Supplementary material associated with this article can be found, in the online version, at doi:10.1016/j.cclet.2025.112068.

References

[1] R. Zhang, M. Chen, Z. Xiong, Y. Guo, B. Lai, Chin. Chem. Lett. 33 (2022) 948–952.
[2] Y. Sun, P. Zhou, B. Lai, et al., ACS Catal. 14 (2024) 6525–6534.
[3] D.Y. Xing, X.D. Zhao, C.S. He, B. Lai, Chin. Chem. Lett. 35 (2024) 109436.
[4] T. Liu, J. Chen, N. Li, et al., Environ. Sci. Technol. 56 (2022) 1300–1309.
[5] S. Correa-Sanchez, G.A. Peñuela, J. Water Process. 49 (2022) 102986.
[6] J. Kim, C.H. Huang, ACS ES&T Water 1 (2021) 15–33.
[7] M. Cai, P. Sun, L. Zhang, C.H. Huang, Environ. Sci. Technol. 51 (2017) 14217–14224.
[8] L. Zhang, J. Chen, Y. Zhang, et al., Water Res. 216 (2022) 118322.
[9] S.Y. Yu, Z.H. Xie, X. Wu, et al., Chin. Chem. Lett. 35 (2024) 108714.
[10] J. Yang, S. Wang, X. Luo, Z. Yu, Y. Zhou, Chin. Chem. Lett. 36 (2025) 110996.
[11] J. Kim, P. Du, W. Liu, et al., Environ. Sci. Technol. 54 (2020) 5268–5278.
[12] P. Hu, M. Long, Appl. Catal. B: Environ. 181 (2016) 103–117.
[13] Y. Zhu, R. Zhu, Y. Xi, et al., Appl. Catal. B: Environ. 255 (2019) 117739.
[14] J. Wang, J. Tang, J. Mol. Liq. 332 (2021) 115755.
[15] G. Li, C. Yang, Q. Yang, et al., Chin. Chem. Lett. 37 (2026) 111207.
[16] C. Lai, X. Shi, L. Li, et al., Sci. Total Environ. 775 (2021) 145850.
[17] Y. Zhang, P. Zhou, B. Lai, et al., J. Hazard. Mater. 443 (2023) 130386.
[18] S. Meng, M. Sun, B. Lai, et al., Environ. Sci. Technol. 57 (2023) 12534–12545.
[19] J. Kim, T. Zhang, W. Liu, et al., Environ. Sci. Technol. 53 (2019) 13312–13322.
[20] S. Li, J. Zou, J. Wu, et al., Environ. Sci. Technol. 59 (2025) 10608–10619.
[21] E.V. Rokhina, K. Makarova, E.A. Golovina, H. Van As, J. Virkutyte, Environ. Sci. Technol. 44 (2010) 6815–6821.
[22] Z. Wang, W. Qiu, S.Y. Pang, et al., Environ. Sci. Technol. 56 (2022) 1492–1509.
[23] C. Dai, S. Li, Y. Duan, et al., Water Res. 216 (2022) 118347.
[24] H. Guo, Y. Wang, J. Wang, S. Tang, T. Wang, Chin. Chem. Lett. 37 (2026) 111275.
[25] X. Qian, M. Ren, M. Fang, et al., Appl. Catal. B: Environ. 231 (2018) 108–114.

[26] M. Ao, J. Wei, B. Lai, et al., Chin. Chem. Lett. 36 (2025) 109882.
[27] H. Wang, L. Gao, Y. Xie, G. Yu, Y. Wang, Water Res. 244 (2023) 120480.
[28] H. Zhang, C. Xie, L. Chen, J. Duan, F. Li, W. Liu, Water Res. 229 (2023) 119392.
[29] Y. Zong, L. Chen, Y. Zeng, et al., Environ. Sci. Technol. 57 (2023) 9394–9404.
[30] X. Lu, W. Qiu, J. Ma, et al., Chem. Eng. J. 401 (2020) 126128.
[31] S. Miyamoto, G.R. Martinez, M.H.G. Medeiros, P. Di Mascio, J. Am. Chem. Soc. 125 (2003) 6172–6179.
[32] D. Xing, S. Shao, Y. Yang, et al., Water Res. 222 (2022) 118930.
[33] S.C. Mei, L. Li, G.X. Huang, X.Q. Pan, H.Q. Yu, Water Res. 241 (2023) 120151.
[34] P. Zhou, J. Zhang, Z. Xiong, et al., Appl. Catal. B: Environ. 265 (2020) 118264.
[35] S.Y. Yu, Y. Shi, B. Lai, et al., J. Hazard. Mater. 462 (2024) 132760.
[36] X. Lu, Y. Yue, S. Deng, et al., Environ. Sci. Technol. 59 (2025) 14170–14181.
[37] Z.H. Xie, C.S. He, B. Lai, et al., Environ. Sci. Technol. 56 (2022) 8784–8795.
[38] L. Wang, J. Wei, J. Huo, et al., Appl. Catal. B: Environ. 371 (2025) 125284.
[39] F. Miao, X. Yue, C. Cheng, et al., Water Res. 227 (2022) 119346.
[40] Y. Lü, J. Li, Y. Li, et al., Appl. Catal. B: Environ. 242 (2019) 9–18.
[41] P. Du, J. Wang, G. Sun, L. Chen, W. Liu, Water Res. 212 (2022) 118113.
[42] M. Chen, T. Yang, Q. Lei, et al., Angew. Chem. Int. Ed. 64 (2025) e202416921.
[43] L. Zhang, J. Chen, Y. Zhang, et al., Appl. Catal. B: Environ. 297 (2021) 120475.
[44] J. Peng, H. Zhou, B. Lai, et al., Chem. Eng. J. 397 (2020) 125387.
[45] R.E. Pearce, G.R. Vakkalagadda, J.S. Leeder, Drug. Metab. Dispos. 30 (2002) 1170–1179.